Solar Energy xxx (xxxx) xxx

Contents lists available at ScienceDirect

Solar Energy

journal homepage: www.elsevier.com/locate/solener

Concentrating Photovoltaic/Thermal Evacuated Glazing (CoPVTEG); Introduction and computational analysis

Mohammad Ghoraishi *, Trevor Hyde *, Aggelos Zacharopoulos, Jayanta Deb Mondol, Adrian Pugsley

Centre for Sustainable Technologies, Belfast School of Architecture and the Built Environment, Ulster University, 2-24 York Street, Belfast, BT15 1ED, Northern Ireland, UK

ARTICLE INFO

Keywords:
Concentrating
Photovoltaic
Thermal
Vacuum
Evacuated
Glazing
Solar
BIPV
STPV
PVT

ABSTRACT

This paper introduces an enhanced version of Concentrating Photovoltaic Glazing (CoPVG) device. The original CoPVG system was designed as a seasonal glazing, that concentrates sunlight onto the focus of the lens during summer. Whilst, in winter, the system transmits light for indoor daylighting purposes. The newly developed version, entitled Concentrating Photovoltaic/Thermal Evacuated Glazing (CoPVTEG), is capable of simultaneously harvesting thermal energy and electricity while vacuum glazing (VG) has been integrated into the device.

A finite element method was employed to simulate the glazing computationally. The developed model was validated by conducting experiments verifying that the model predicts the glazing performance reliably.

Two different configurations were considered: placing the VG facing either outside, called disposition A, or inside, called disposition B. These dispositions were analysed computationally to determine the thermal and electrical output powers of the device in Belfast, UK. It was found that locating the VG inside potentially doubled the output electrical power ranging from 63.32 W/m^2 to 92.56 W/m^2 and from 36.03 W/m^2 to 43.88 W/m^2 at noon throughout the year for disposition B and A, respectively. However, the thermal harvesting potential of disposition A is higher than disposition B. In this case, the device potentially generates from 216.46 W/m^2 to 406.20 W/m^2 thermal power at noon. While the potential will be reduced from 163.54 W/m^2 to 396.11 W/m^2 in disposition B. Disposition A is more advantageous for cold-dominant climate zones while disposition B is the suggestion for temperate climate zone like the studied case.

1. Introduction

The increasing apprehension regarding greenhouse gas emissions and the consequential impact of climate change on human life has prompted a motivation to enhance energy efficiency across all sectors globally. For example, in 2008, the United Kingdom enacted the Climate Change Act [1], to tackle the problem. This plan has since been promoted by the Net Zero Strategy (NZS), launched in 2021, with the aim of achieving net zero greenhouse gas emissions by 2050 [2]. To achieve this ambitious goal, the country has aimed to augment the proportion of renewable energy and improve energy efficiency in all demand sectors, including the building sector which accounts for over 30% of total energy consumption in the country [3].

Renewable energy technologies, such as Building Integrated Photovoltaic (BIPV) and Building Integrated Photovoltaics/Thermal (BIPV/T) systems, have been developed to enhance the energy performance of buildings by harnessing solar-based energy [4]. BIPV is intended to replace conventional building external envelopes [5]. With low U-values, BIPVs provide not only passive energy-related functions but also the ability to generate benign electricity. In the case of BIPV/T systems, thermal energy generation is also incorporated.

These devices emerge in the fenestration part of buildings as Semi-Transparent Photovoltaic (STPV) and Semi-Transparent Photovoltaic/Thermal (STPV/T) glazing devices, respectively. While regulating room illuminance, and preventing excessive glare, therefore, limiting heat gain, they generate electricity and heat [5]. There has been increased interest in the devices aiming to improve the energy performance of buildings by utilizing the aforementioned facades that are multifunctional and energy efficient. Following this context, a review of the recent investigations is presented.

As an example, an experimental and simulative study was conducted on a novel Concentrator-Photovoltaic Window (CPVW) which provides uniform daylighting in Ref. [6]. The inside lighting uniformity was

* Corresponding authors.
E-mail addresses: ghoraishi-m@ulster.ac.uk (M. Ghoraishi), t.hyde@ulster.ac.uk (T. Hyde).

https://doi.org/10.1016/j.solener.2023.111814
Received 22 March 2023; Received in revised form 29 May 2023; Accepted 22 June 2023

compared with the relevant spaced STPV window. It was concluded that CPVW is able to collect and scatter sunlight more effectively than traditional STPV glazing.

A new type of window called the asymmetric concentrator-photovoltaic type window has been proposed in Ref. [7]. This window can efficiently generate electricity while also providing natural daylight. It was discovered analytically that the asymmetric concentrator can achieve an optical efficiency of above 80% in a broad acceptance range of 10°–85°.

A novel Photovoltaic (PV) glazing called 3D concentrating PV was reported in Ref. [8]. Tests have demonstrated that the modules can raise the maximum power output by 2.89 times, and they also provide consistent interior daylighting with a transmittance of 9.47%.

Building Integrated Concentrating Photovoltaic (BICPV) smart window combines optically switchable thermotropic layers with integrated PV cells to enable the simultaneous generation of electricity and the regulation of solar heat and visible light in buildings [9]. The study discovered that the BICPV smart window potentially increases the maximum power output by 17.1%. However, as the temperature increases, the window's light transmittance decreases by 70.9%.

As an example of BIPV/T, Ref. [10] computationally and experimentally investigate Natural Ventilated Double PV (NVDPV) windows. The NVDPV window has a design with two air vents located at the top and bottom on both sides of the window for regulating air from outside or inside in summer or winter, respectively.

Also, the research reported in Ref. [11] investigates an integrated STPV/T on Double Skin Facades (DSF) to regulate solar heat and produce electrical energy. Under various experimental conditions, the heat recovery index can exceed 30%, while the overall solar utilization efficiency can range from 30% to 77% in both generating electricity and heat.

Furthermore, the energy performance of a PV Double Skin Façade (PV-DSF) and a PV Insulating Glass Unit (PV-IGU) was evaluated through comparative experiments to determine their respective efficiencies in Ref. [12]. The PV-DSF system is composed of three main layers, including a semi-transparent amorphous Silicone (a-Si) PV panel located on the outer layer, a glass sheet on the inner layer, and an intermediate air ventilation cavity which removes waste heat from the PV modules. The PV-IGU system comprises an outer layer of STPV, an air gap, and an inner layer of glass. The air sealed in the air gap provides increased thermal insulation performance for the window. The latter system can be used in building retrofit projects, also. According to the findings, the PV-DSF and PV-IGU systems have demonstrated average energy-saving potentials of 28.4% and 30%, respectively.

According to Ref. [13], the use of PV glazing can reduce heat gain by reducing radiative transmittance. However, Ref. [14] indicates that this type of glazing may increase the building's cooling load because of the wasted heat from the PV phenomenon. To address the issue, a combination of PV glazing with vacuum glazing (VG), which is an effective thermal insulating glazing façade component [15], is proposed in Ref. [14] that may mitigate the problem. In their study, a four-layer glass system bonding PV glazing and VG was proposed to achieve a low U-value semi-transparent façade while generating electricity from the glazing.

Other research teams have also examined the integration of PV glazing and VG. For instance, Vacuum Photovoltaic Insulated Glass Unit (VPV IGU) was developed and investigated in Ref. [16] that utilizes semi-transparent a-Si PV cells. They concluded that vacuum PV glazing presents significant potential for energy savings in regions characterized by severe cold, cold, hot summer and cold winter, and hot summer and warm winter climates. However, the device may not be suitable for moderate climatic regions.

Further investigation on VPV IGU was conducted in Ref. [17]. The comparative study has demonstrated the thermal insulation capabilities of VPV IGU, as it is capable of reducing heat gain by as much as 81.63% and 75.03% in Hong Kong (HK) and Harbin (HB), respectively. Moreover, VPV IGU is shown to decrease heat loss by 31.94% and 32.03% in HK and HB, respectively.

Also, a four-layer PV VG system (PV-VG 4L) was reported in Ref. [18] and subsequently, the research group explored a lighter and thinner design (PV-VG 2L) in which the PV cells are placed inside the vacuum gap [19]. By means of a verified mathematical model, the performance of PV VG-2L was numerically simulated at its optimal design, revealing an average U-value as low as 0.60 W/m^2 K. However, the electricity generation was reported from 200 mW to 400 mW per 0.3 m by 0.3 m prototype in an average of 600 W/m^2 solar irradiance.

Moreover, a three-glass layer system featuring spaced opaque crystalline-Silicone (c-Si) PV cells [20], also, a three-layer system combining a semi-transparent PV cell made of Cadmium Telluride (CaTe) [21] with VG were both investigated. Ref. [20] concluded that integrating VG with BIPV enhanced the thermal comfort of the building occupant by 39% when compared with the relevant BIPV. Ref. [21] employed an Artificial Neuron Network (ANN) coupling method to investigate the effect of the three-layer vacuum CaTe PV glazing on lighting consumption concluding that the ANN model is more efficient and accurate in predicting illuminance values.

Finally, a concentrating STPV glazing concept was introduced in Ref. [22]. The glazing has been investigated at Ulster University. The fundamental form of the idea is called Concentrating Photovoltaic Glazing (CoPVG) [23]. An academic study has demonstrated that the use of CoPVG lenses has the potential to increase the electrical output power of glazing by approximately 5% to 8%, as well as by approximately 46% to 52% during winter and summer seasons, respectively, when compared to conventional STPV glazing with the same opaque area percentage [24].

To increase the U-value of the glazing and its thermal energy collection capacity, an additional glass pane may be added to the outer surface [25]. When the gap is evacuated, the version is known as Concentrating Photovoltaic Evacuated Glazing (CoPEG) [26]. Another variation of the glazing was constructed with an inner glass pane that forms a cavity behind the lenses. Forced air flows through the cavity producing hot air and lowering the temperature of the PV cells. This version is called Concentrating Photovoltaic/Thermal Glazing (CoPVTG) [26].

STPV units have the potential to generate electricity and reduce glare. However, previous studies have shown that PV cells can increase the glazing temperature to uncomfortable levels, especially when VG is integrated [5]. Despite this, VG is beneficial for energy conservation in buildings due to its thermal insulation properties. STPV/T systems are beneficial to exploit the wasted heat and have the potential to overcome the discomfort.

The current paper aims to figure out the interaction between VG and the energy harvesting potential of CoPVTG. Entitled Concentrating Photovoltaic/Thermal Evacuated Glazing (CoPVTEG), a new configuration of the CoPVG concept is introduced. Table 1 provides an overview of various glazing devices reviewed in the context and their corresponding functionalities illustrating the superiority of CoPVTEG device over previously developed ones. The device is investigated computationally with an experimentally validated model utilizing Finite Element Method (FEM).

2. Concept introduction and simulation approach

The CoPVG system is composed of several longitudinal prismatic lenses. Fig. 1 illustrates a cross-sectional view of the glazing and depicts the system's response to radiation beam directions. As illustrated in the figure, the device concentrates solar radiation on the focal area of the glazing, where PV cells are attached, in summer when the sun is high in the sky. This results in higher electrical power output while also shading and reducing heat gain [23]. Conversely, the glazing partially transmits sunlight to the indoor environment for room daylighting purposes during winter. The CoPVG lens is designed to adjust the

Table 1
CoPVTEG functionality comparison.

Functionality	CoPVTEG	CoPVTG	CoPEG	CoPVG	STPV	CPVW [6]	Asy. CPV [7]	3D CPVD [8]	BICPV [9]	NVDPV [10]	PV-DSF [11]	PV IGU [12]	VPV IGU [14]	PV-VG 4L [18]	PV-VG 2L [19]
Seasonal solar gain control	✓	✓	✓	✓											
PV electricity generation	✓	✓	✓	✓	✓	✓	✓	✓	✓	✓	✓	✓	✓	✓	✓
Solar concentration	✓	✓	✓	✓		✓	✓	✓							
Daylighting and glare control	✓	✓	✓	✓	✓	✓	✓	✓	✓	✓	✓	✓	✓	✓	✓
Thermal energy harvesting	✓	✓								✓	✓				
Enhanced thermal insulation	✓		✓							✓		✓	✓	✓	✓

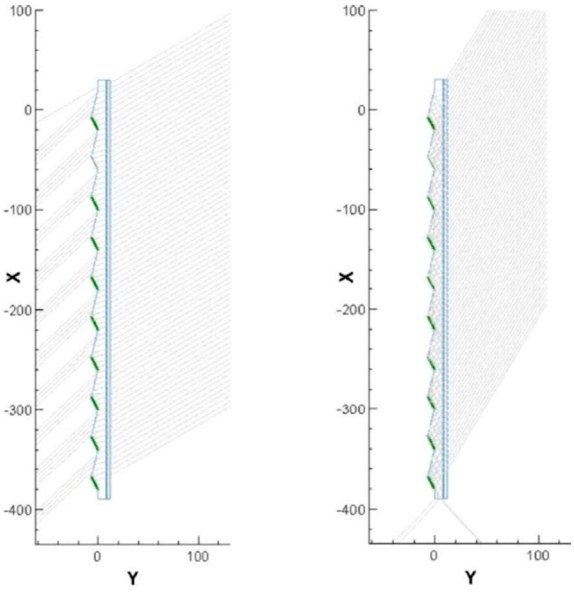

Fig. 1. Ray trace diagrams for incident angles of 20° (left) and 55° (right) from the normal vector of the glazing surface in the CoPVG device [23].

glazing functionality against to the sun's location in the sky and can be customized according to the building's location. The authors have investigated the optical performance of the lenses and presented their findings elsewhere [24].

The CoPVTEG concept comprises the CoPVG and an additional glazing layer on the rear side of the lenses, which creates a cavity. Air is blown through the cavity that acts as the heat-exchanging fluid to absorb wasted heat from the PV cells. Furthermore, the device is integrated with a VG unit to improve its thermal resistance. Two configurations are possible, depending on whether the VG is placed facing outward, called disposition A, or inward, called disposition B. Fig. 2 depicts these dispositions. In the former case, a simple glass pane at the rear side is required to create the cavity which is substituted by VG in the latter case.

Selecting the configuration of the CoPVTEG system involves a trade-off between higher thermal energy harvesting potential and higher electricity production in disposition A and disposition B, respectively. Disposition A, in which the VG faces outward, provides higher thermal energy harvesting potential due to lower heat loss through the outside layer. In contrast, disposition B, in which the VG faces inward, yields greater electricity production due to lower solar absorption through the outside layer, while radiation intensity on the PV cells will be reduced further in disposition A due to the radiative absorptivity of the VG and internal reflections caused by the additional surfaces.

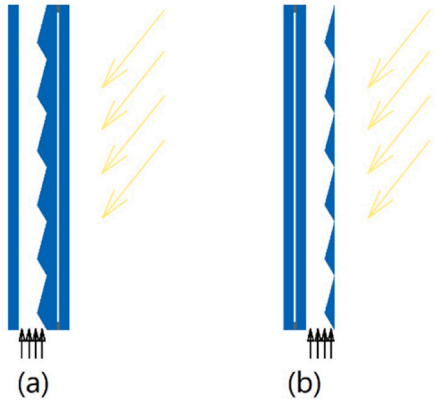

Fig. 2. Concentrating photovoltaic/thermal evacuated glazing dispositions; (a) Disposition A, (b) Disposition B.

The science of Computational Fluid Dynamics (CFD) is often employed to predict fluid heat and mass transfer using a set of interconnected equations to solve for mass and energy conservation. Therefore, CFD has been utilized in this study to understand the performance of the conceptual devices. The advantage of using CFD is that it reduces the reliance on experimental studies. Nevertheless, experimental studies are still required to validate the model and findings.

STPV/T systems harvest both electrical and thermal energy through the glazing unit. Therefore, the primary objectives of the computational study are to evaluate the electrical and thermal output power of CoPVTEG devices. Additionally, the computational study aims to provide a comprehensive understanding of the concept, including airflow patterns and temperature distribution within the domains and boundaries. The model will be utilized for a broad investigation of design modifications and optimization which will be presented in the subsequent papers. In this research, the computational model is employed to investigate the significance of incorporating VG and CoPVG devices.

Solar utilization efficiency of CoPVTEG is influenced by various factors, including; building location, glazing orientation, ambient conditions, time, weather conditions, and physical properties of the glazing components. However, this investigation aims to compare the solar utilization efficiency of CoPVTEG based solely on the glazing's configuration, irrespective of other factors. To evaluate the solar utilization efficiency of the device, a heat transfer analysis was conducted. The diagram in Fig. 3 illustrates the conductive, convective, and radiative heat transfer through the glazing unit. It is worth noting that the outside and inside glass panes are substituted with their physical properties at the boundaries.

Utilizing the Finite Element Method (FEM), a model was developed in ANSYS to investigate the energy performance of CoPVTEG. The model comprises four external boundaries: outside, inside, and the

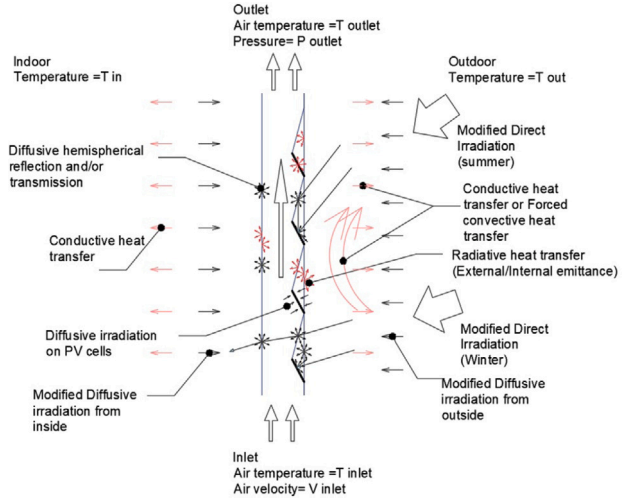

Fig. 3. Schematic diagram of radiation and total heat transfer through CoPVG systems.

cavity's inlet and outlet. The outside boundary conditions include; solar directive and/or diffusive irradiation, emissivity, outdoor temperature, and forced convective heat transfer from the glazing surface in disposition B or the thermal resistance (U-value) of the VG layer in disposition A. The inside boundary condition is determined by; the indoor temperature, the U-value of the inside glazing layer, emissivity, and diffuse irradiation. Air is blown through the cavity, so the air velocity and temperature are considered the inlet boundary conditions. The outlet boundary is determined by the pressure and temperature.

It is crucial to optimize the computational model by reducing the number of elements while maintaining a reasonable level of accuracy. To achieve this goal, four measures and assumptions were taken. First, the airflow within the cavity was assumed to be uniform across the width of the glazing. Second, the electrical and thermal performance of the PV stripes bonded on each longitudinal lens was assumed to be uniform along the lens focus. Third, the inside and outside glass layers were excluded from the simulation, and their conductive and radiative heat transfer properties were replaced in the model. Last, to make the computational efforts more practical, only a vertical slice of the glazing was modelled, so, radiation was assumed to be transitional from the sides of the slice. However, the last assumption neglects the impact of the edges of the CoPVTEG system.

The electrical output power of PV cells is calculated by multiplying the total incident irradiation on the PV surfaces and the efficiency of the PV cells at the operating temperature. In the context of CoPVG systems and their electricity generation, the gross electrical power production (P_{PV}) is determined by Eq. (1) [25].

$$P_{PV} = \eta_{PV} \cdot I \cdot s \tag{1}$$

where, η_{PV} represents the efficiency of the PV system, I denotes the incident surface radiation, and s is the PV cell surface area.

To ensure energy balance within the system, the influence of the electrical power collection within the PV cell domains is modelled as a negative heat source acting within the volumetric regions of the PV cells. The negative heat source represents the dissipation of heat due to the conversion of solar energy into electricity within the PV cells. Considering Eq. (1), the volumetric negative heat source is quantified by Eq. (2).

$$S_{wall} = -\frac{\eta_{PV} \cdot I \cdot s_i}{s_i \cdot t_{PV}} = -\frac{\eta_{PV} \cdot I}{t_{PV}} \tag{2}$$

where, s_i denotes the surface area of the ith PV cell surface element and t_{PV} represents the thickness of the PV cells. The incident surface radiation, I, is an unknown parameter that is calculated within the model at each PV surface element.

The PV cell efficiency, η_{PV}, is considered to decrease linearly as the operating temperature increases [27] and is calculated by Eq. (3).

$$\eta_{PV} = \eta_0 - c(T_{PV} - 25\ ^\circ\mathrm{C}) \tag{3}$$

Therefore, the PV cell standard efficiency, η_0, the temperature coefficient of the PV cell, c, and the PV cell efficiency at operating temperatures, η_{PV}, which is calculated by solving the interconnected equations for evaluating PV cell operating temperature, T_{PV}, are also included in the calculation of S_{wall}. S_{wall} [W/m^3] is computed for each PV cell surface element and simulated accordingly.

The primary outputs of the simulation are the outlet air temperature, the thermal output power, and the electrical output power. The outlet air temperature is calculated by mass weighted average air temperature at the outlet boundary. The thermal output power is the heat transfer rate by the air entering and exiting the fluid domain from the inlet and outlet boundaries, respectively, and is basically derived from energy conservation. The electric output power is the summation of the gross electricity power generation calculated by Eq. (1) at the PV cell surface boundaries. These parameters are formulated by the Eqs. (4), (5), and (6), respectively.

Outlet air temperature:

$$T_{Outlet} = \frac{\sum_{Outlet} m_i T_i}{\sum_{Outlet} m_i} \tag{4}$$

Thermal output power:

$$P_{Th} = -\frac{l}{t}\left(\sum_{inlet} \dot{Q} + \sum_{outlet} \dot{Q}\right) \tag{5}$$

Electrical output power:

$$P_E = \frac{l}{t} \sum_{PV\ surface} \eta_{PV} I s_i \tag{6}$$

In the above equations, m_i and T_i denote the mass and temperature of the air passing through the ith finite surface at the boundary. The $\frac{l}{t}$ parameter represents the model geometry correction which is obtained by dividing the length of the glazing by the thickness of the modelled slice, and $\dot{Q}$ refers to the heat transfer rate.

To computationally compare the configurations, a case is defined and both dispositions are simulated under identical conditions. The glazing was simulated for a building located in Belfast, UK, with the outward face towards the south. No sunlight-obstructing obstacles are assumed. The simulation calculates the glazing performance for the 21st of every month at noon, assuming clear skies and maximum theoretical radiation at the times. The outside temperature is assumed to be the average daily high temperature, and the wind speed is held constant, resulting in a convective heat transfer rate of 25 W/m^2 K from the outside surface of the glazing. The inside temperature is kept constant at 20 °C throughout the year.

To ensure the accuracy of the simulation, the model was validated experimentally in advance. The validation experiments are presented in the following section, followed by the presentation of the simulation results.

3. Model validating experiments

The computational model is a cost-effective method for studying CoPVTEG systems. The model can also be utilized in the detailed design and optimization of the CoPVG devices. However, to ensure its accuracy, the model needs validation. This section focuses on the attempts made to validate the computational model. To achieve this, a CoPVTG prototype was constructed and mounted on a rig that could be adjusted for various conditions. The glazing was then exposed to radiation from a solar simulator at the Centre for Sustainable Technologies (CST), Ulster University. The same scenarios as the experimentations were

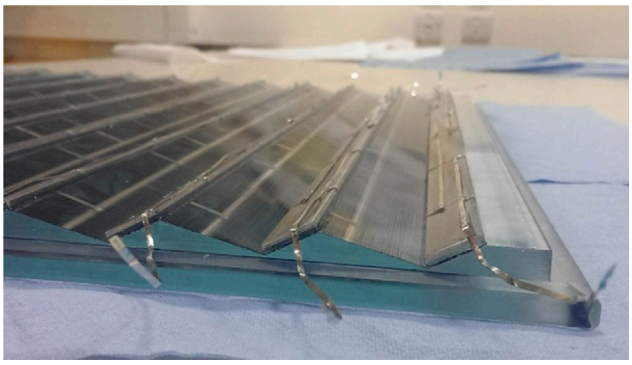

Fig. 4. Inside of the traditional CoPVG [25].

simulated in the model. Then, comparing the results led to model reliability analysis. The evaluated model has been adapted for analysing CoPVTEG systems, replacing the thermal and optical characteristics of VG in boundaries. This section is divided into two subsections that describe the fabrication and experimentation processes.

3.1. Prototype fabrication

In general, two methods are used to create CoPVG systems. The first approach involves cutting a complete lens from a thick glass pane that is at least 15 mm thick and then shaping it to form the desired concentrating lines. PV cell strips are then attached to the focal point of the lens. The second approach involves cutting and polishing individual lenses and then attaching PV cell strips to each lens. The PV-laminated lenses are then assembled modularly onto a glazing frame.

Earlier studies on the first method were successful in creating and testing the CoPVG and CoPEG concepts, as explained elsewhere [23,25]. However, producing lenses with purely spectral surfaces was found to be challenging. The cutting process can result in some lines on the lens surface, as shown in Fig. 4, which can reduce the transparency and optical efficiency of the glazing. Nonetheless, the lines can be improved by either refining the cutting techniques and wheels or by covering them with silicon. However, since the entire lens is made up of a relatively thick glass layer, about 8 mm beyond the prism in the aperture, this can lead to a decrease in irradiation intensity on the focus and an increase in weight.

Fig. 5 illustrates the design and examples of PV-laminated individual lenses produced using the second approach. This method offers several advantages, including:

- Reduced risk of involving lenses with non-conforming quality since failed lenses can be easily detected using an I-V curve tracer before continuing with the production process.
- Creation of individual lenses with a nearly purely spectral surface, resulting in better optical performance as a concentrator.
- Requirement of less material for the individual lens approach, making the final product potentially lighter and more cost-effective.
- Less complexity in the production of individual lenses compared to whole lenses due to the simple geometry, resulting in a less expensive glazing system.
- Potential to generate more electrical power as a result of lower radiation absorption by the lens.
- Flexibility in the installation of individual lenses in various architectural designs due to the product's modular system.
- Integration of individual lenses into existing buildings is possible.

To fabricate the CoPVTG prototype that will be used to validate the computational model, a wooden frame was designed and constructed. Then, the PV-laminated individual lenses are mounted on the frame followed by establishing connections and sealing gaps. The prototype is depicted in Fig. 6.

3.2. Experimentation

This subsection describes the efforts undertaken to characterize the thermal and electrical performance of the prototype under a set of predefined scenarios.

The prototype underwent experimental evaluation at CST of Ulster University under an advanced indoor solar simulator facility. This facility employs a state-of-the-art configuration comprising 35 high-power metal halide lamps arranged in 7 rows, with each row containing 5 lamps. Each lamp is equipped with a rotational symmetrical paraboloidal reflector to achieve precise and concentrated illumination, resulting in a highly collimated light beam. Additionally, a lens is inserted into each lamp to ensure uniform distribution of light intensity across the testing area, effectively expanding the illumination coverage. The combined features of the reflector, lens, and lamps enable an accurate simulation of the beam path, spectrum, and uniformity.

The rationale behind conducting the tests indoors was to assess the model's output in controlled, steady-state conditions, which cannot be easily achieved in an outdoor setting. Outdoor tests are susceptible to variations caused by the continuously changing position of the sun in the sky and unpredictable weather conditions that may fluctuate throughout the duration of the experiment. To ensure the accuracy and reliability of the experimentation, the decision was made to perform the tests indoors.

To do so, the prototype was installed on a rig designed to maintain the indoor face of the prototype at desired temperatures while exposing the outdoor face to the solar simulator at various altitude angles from 10 to 70 degrees in 20-degree intervals. These angles were chosen to represent different positions of the sun throughout the year. However, the tests were intentionally classified into summer or winter scenarios to highlight the seasonal effect of the prototype as described in Section 2. The diagram of the rig is depicted in Fig. 7, while Fig. 8 shows the rig itself.

The temperatures at several points, including inlet and outlet air, were measured by T-type thermocouples to evaluate thermal power and validate the relevant outputs from the model. Additionally, the electrical output power was measured using a DayStar DS-1000 I-V curve tracer at steady-state conditions, while an electric load had been connected to collect electricity during the test. An EA-EL 9080-45 T, DC Electronic Load device manufactured by EA Elektro-Automatik was used as the electric load.

In winter scenarios, the temperature within the box representing the indoor environment was kept higher than the lab temperature, which represents the outside environment for the glazing. Additionally, the incident angle was kept below a critical angle in these scenarios due to the sun's altitude during winter. The critical angle is the angle at which the functionality of the glazing changes from room lighting to shading by increasing the altitude angle which is 37° at azimuth zero for the individual lenses [24]. In summer scenarios in contrast, the box temperature was kept lower than the room temperature due to the lower indoor temperatures in summer, while the incident angles were adjusted to be above 50°. To maintain the temperature of the hot/cold box, a refrigerated circulator device manufactured by JULABO was used. Fig. 9 shows the experimentation for a winter scenario when the irradiation beam made an angle of 30° with the glazing normal vector.

To evaluate the computational model's reliability, ten independent scenarios were simulated. The details of these scenarios are summarized in Table 2. The same scenarios were replicated in the computational model to enable the comparison of the results.

Table 2
Test scenarios and the relevant input parameters for the evaluation tests.

	Test ID	Incident angle [Deg]	Inlet air velocity [m/s]	Inlet air temp [°C]	Cold/Hot box temp [°C]	Room temp [°C]	Irradiation intensity on the glazing surface [W/m^2]
Winter scenarios	10.1	10	1.7	28.2	48.4	24.4	780
	10.2	10	1.5	41.1	48.7	23.8	780
	30.1	30	1.9	29.2	47.8	26.2	555
	30.2	30	1.5	42.2	47.9	26.5	555
	30.3	30	1.7	30.3	47.9	28.8	555
	30.4	30	1.4	39.9	48.1	28.3	555
Summer scenarios	50.1	50	1.8	25.7	10.1	24.0	364
	50.2	50	1.5	21.0	11.2	24.7	364
	70.1	70	1.7	24.9	9.8	23.7	246
	70.2	70	1.5	20.6	11.4	23.9	246

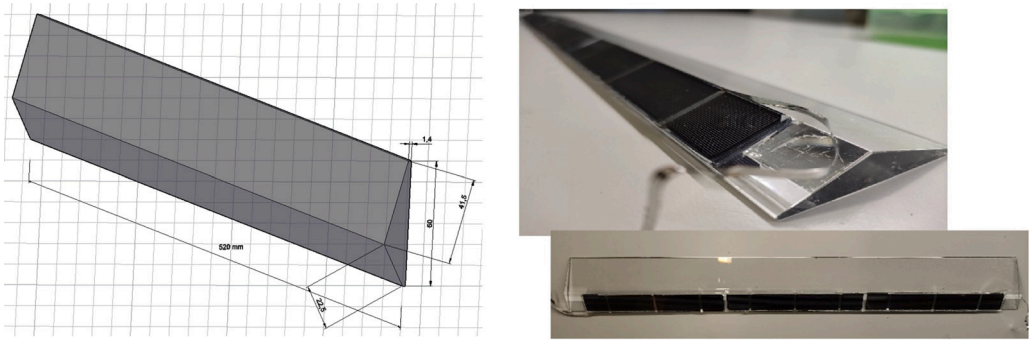

Fig. 5. The geometry of the individual lenses and samples of the final product of the PV-laminated lens. Dimensions are mentioned in millimetres.

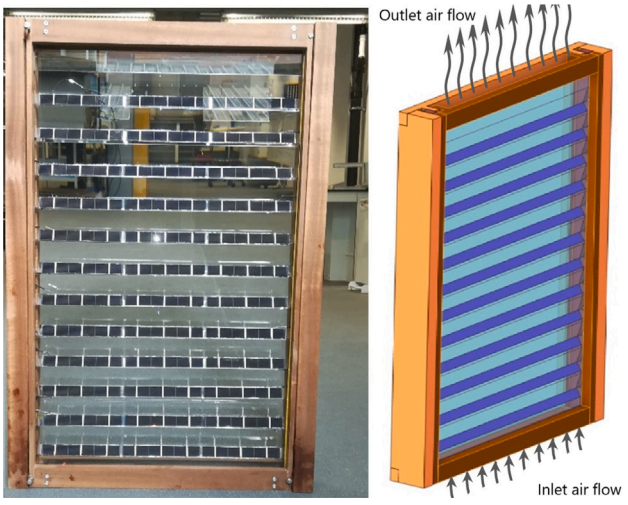

Fig. 6. The CoPVTG prototype fabricated with the individual lenses.

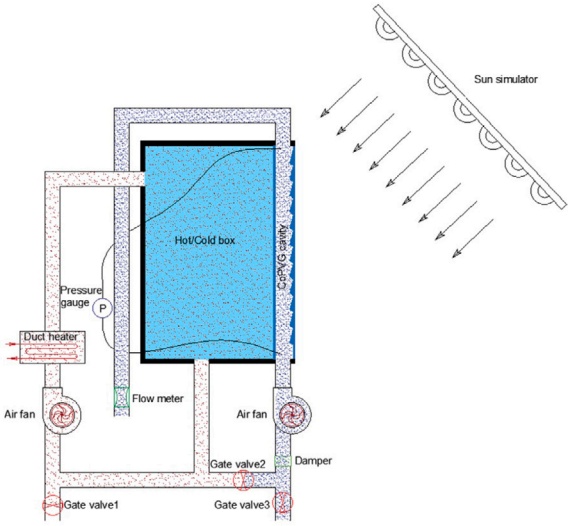

Fig. 7. The diagram of the mechanical aspect of the rig.

4. Results

4.1. Model evaluation

Table 3 displays a comparison between the output parameters obtained from the experiments and the corresponding values predicted by the model. The output parameters include the electrical output power generated by the device, as well as the temperature of the outlet air and five additional checkpoints. The first three checkpoints are located at the rear side of the PV strip rows numbers five, eight, and eleven, respectively, arranged in ascending order from the bottom to the top of the glazing. The final two checkpoints are positioned within the cavity and on the rear glass panel at one-third and two-thirds of the glazing height, respectively. With regards to the electrical output power, the greatest deviation between the model predictions and experimental results was observed at the altitude of 30° which is close to the critical angle. This deviation is attributed to the use of a solar simulator equipped with a multi-lamp system. As illustrated in Fig. 9, rays emanating from the lamps positioned at the uppermost rows may exceed the critical angle and thereby focus on the PV cells. Consequently, the electrical power output measured in the experiments was found to surpass the predicted values of the model. Notwithstanding these observations, the electrical output power data from the experiments aligned with the corresponding model predictions and were consequently employed in the model validation analysis.

In order to assess the accuracy of the model in predicting temperature and thermal performance, an error analysis was conducted,

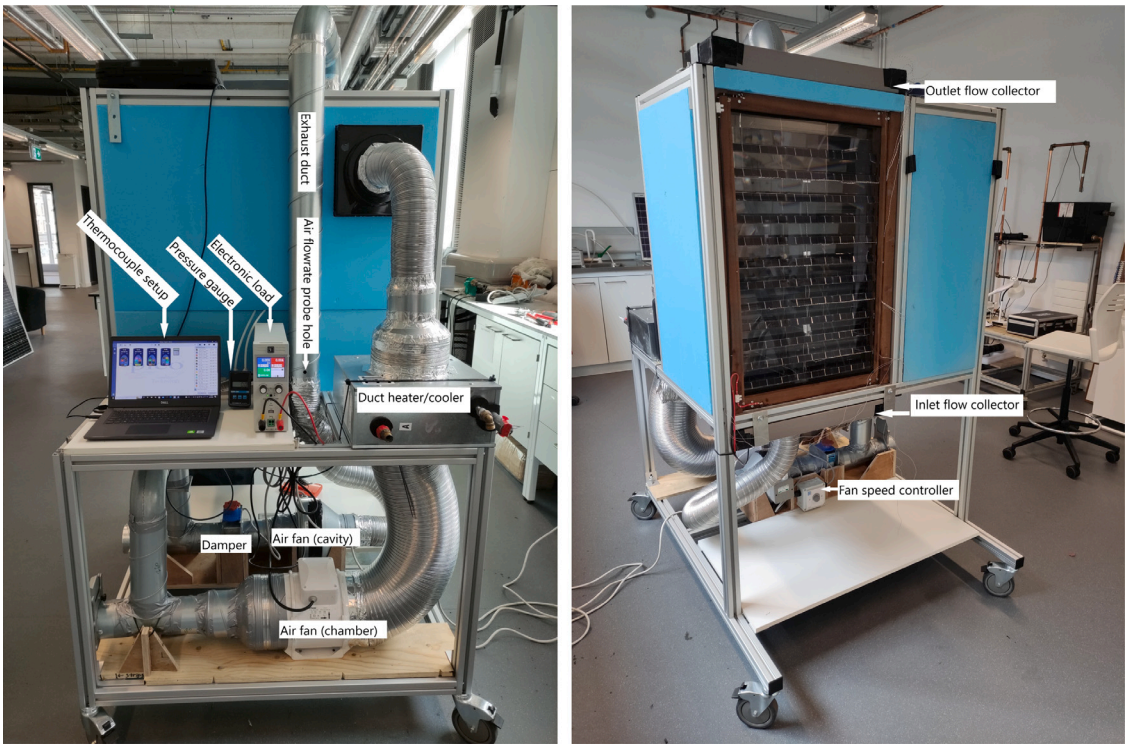

Fig. 8. The experimenting rig.

Table 3
Output parameters from the computational model vs. the experimentally measured values.

Test ID	Output electrical power		Outlet air temp		Temp at checkpoint1		Temp at checkpoint2		Temp at checkpoint3		Temp at checkpoint4		Temp at checkpoint5	
	Exp. [W]	Com. [W]	Exp. [°C]	Com. [°C]	Exp. [°C]	Com. [°C]	Exp. [°C]	Com. [°C]	Exp. [°C]	Com. [°C]	Exp. [°C]	Com. [°C]	Exp. [°C]	Com. [°C]
10.1	14.8	14.8	33.7	33.7	33.3	35.6	35.4	36.6	37.8	37.7	38.2	37.2	39.1	37.6
10.2	14.2	14.0	43.4	43.4	44.5	46.3	45.4	46.8	48.2	47.2	45.5	44.8	45.8	45.0
30.1	13.6	12.3	34.9	33.6	34.0	34.8	35.8	35.6	38.5	36.5	38.5	36.9	39.7	37.3
30.2	13.0	11.6	44.8	43.8	45.0	46.1	45.6	46.4	47.2	46.7	45.5	45.0	45.9	45.1
30.3	13.4	12.1	35.7	35.1	35.5	36.7	37.2	37.6	40.2	38.5	39.3	38.2	40.2	38.6
30.4	13.0	11.6	43.2	42.5	43.6	44.9	44.1	45.5	46.7	45.9	44.6	44.0	45.1	44.3
50.1	13.5	13.2	24.8	26.1	29.0	32.2	32.3	32.3	30.8	32.2	20.3	19.3	20.0	19.8
50.2	13.6	13.3	21.2	23.1	26.2	29.5	29.5	29.9	28.9	30.2	18.0	16.6	17.9	17.3
70.1	8.0	8.4	21.6	24.4	27.6	28.9	28.5	28.8	27.5	28.7	19.2	18.4	18.7	18.7
70.2	8.4	8.5	19.0	21.5	24.8	26.0	26.6	26.1	25.8	26.2	17.6	16.4	17.4	16.9

incorporating the use of residuals and standard errors of the estimate. Table 4 displays the residuals, obtained by subtracting the experimental data from the corresponding model predictions. Table 5 presents the evaluation of the model's reliability in predicting the experimental data, based on the maximum acceptable errors.

It is important to highlight that the predicted temperature values fall within the standard measurement error of the thermocouple, which is ±1 °C, in half of the cases. Additionally, taking into account the measurement errors associated with airflow rate, which directly impact temperature distribution within the domains, suggests that the predicted temperatures closely match the values obtained from the experiment. Nonetheless, it should be noted that all measured data was utilized in the reliability analysis of the model.

The analysis reveals that the model's predictions demonstrate a higher level of agreement with the experimental results concerning electrical performance. This is due, in part, to the relatively straightforward nature of measuring output power experimentally. However, the model's reliability in predicting thermal performance falls to some extent as shown in Table 5, primarily due to the complexity of measuring relevant parameters, such as air flow rate and temperature and these measurements are not as straightforward as those involved in measuring electrical performance. Despite these limitations, the model shows an acceptable level of accuracy and reliability to be adopted for evaluating the CoPVTEG concept.

Table 4
Table of residuals. The model outputs subtracted by the experimentally evaluated data.

Test ID	Electrical Power [W]	Outlet air [°C]	Check points (1) [°C]	(2) [°C]	(3) [°C]	(4) [°C]	(5) [°C]
10.1	0.0	0.0	2.3	1.3	−0.2	−1.0	−1.4
10.2	−0.2	0.0	1.8	1.4	−0.9	−0.6	−0.7
30.1	−1.3	−1.3	0.8	−0.2	−2.0	−1.5	−2.4
30.2	−1.4	−1.0	1.1	0.9	−0.5	−0.5	−0.8
30.3	−1.3	−0.6	1.1	0.4	−1.6	−1.1	−1.6
30.4	−1.4	−0.7	1.3	1.3	−0.8	−0.6	−0.8
50.1	−0.3	1.3	3.1	0.0	1.4	−1.1	−0.2
50.2	−0.3	1.9	3.3	0.4	1.3	−1.4	−0.6
70.1	0.4	2.8	1.3	0.3	1.1	−0.9	−0.1
70.2	0.1	2.5	1.1	−0.5	0.5	−1.2	−0.5

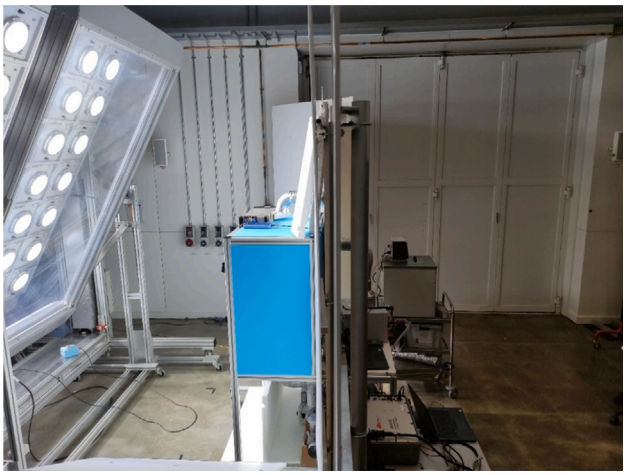

Fig. 9. Prototype experimentation for a winter scenario and an altitude angle of 30°.

Table 5
Table of tolerance-reliability of the computational model.

Maximum acceptable error	Reliability of the model's results for	
	Electrical performance	Thermal performance
1.0%	35.0%	24.0%
2.0%	64.9%	34.4%
3.0%	87.4%	48.6%
4.0%	97.0%	63.5%
5.0%	99.5%	76.5%
6.0%	100.0%	86.3%
7.0%	100.0%	92.7%
8.0%	100.0%	96.5%
9.0%	100.0%	98.5%
10.0%	100.0%	99.4%

4.2. CoPVTEG evaluation

Table 6 provides a summary of the output data obtained from the simulation, encompassing the thermal and electrical output powers for both dispositions in units of watts per square meter of glazing. Additionally, the table reports the outlet air temperature, indicating the point at which the air temperature increases. For interpretation purposes, the sun's altitude and radiation intensity, are also included in the table.

5. Discussions

Fig. 10 illustrates the difference in energy performance between the two CoPVTEG dispositions. The comparison of the two glazing configurations reveals that the placement of VG outwards, disposition A, results in a considerable reduction in electricity generation. However, the thermal output power is higher in this configuration, as anticipated. As a result of the simulation, the total output power of disposition A exceeds that of disposition B, where the VG is placed inward, in all simulation scenarios except for August. In August, when the ambient temperature is as high as the inside temperature, the latter configuration, disposition B, loses less heat through the outside surface and generates nearly as much thermal output power as disposition A. Moreover, the slightly higher thermal output power generated in disposition B than in disposition A in August is due to the greater radiative intensity on the PV cells because of the lower optical thickness.

Disposition A shows a greater degree of consistency in electricity production throughout the year, despite generating only half the power of the other configuration. This consistency is attributed to the interplay between the occurrence of Total Internal Reflection (TIR) and the sun's

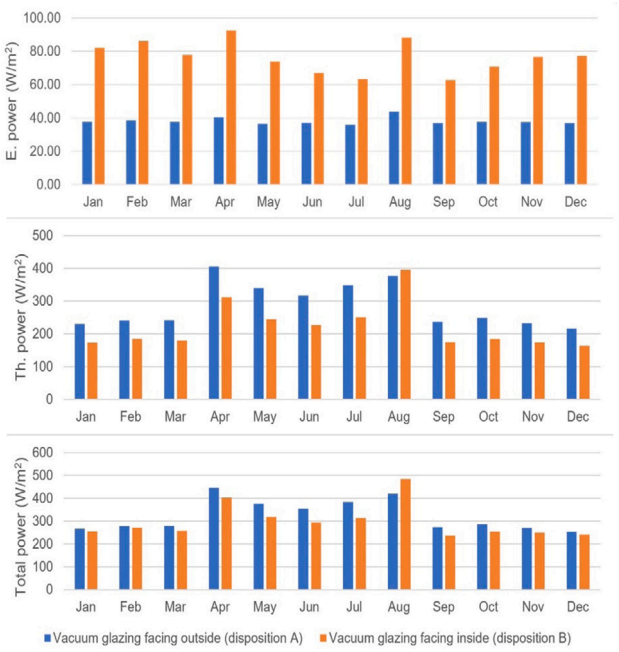

Fig. 10. Dispositions' energy performance comparison.

altitude angle, also the consistency in the operating temperature. To illustrate, during winter months, when the sun's altitude falls below the critical angle of the lens, TIR does not occur. Nevertheless, a relatively high perpendicular component of radiation on the vertical surface of the glazing compensates for the absorbed irradiation at the focus of the lens. In contrast, during summer months, when the altitude angle is high and the perpendicular component of irradiation on the glazing surface falls, the presence of TIR in the lenses compensates for the total irradiation intensity at the focus. Additionally, the operating temperature remains nearly constant at a few degrees above room temperature, resulting in consistency in the PV cell efficiency and, therefore, output power throughout the year. The electrical output power reaches a maximum of 43.88 W/m^2 in August, when the sun's altitude is just above the critical angle, and a minimum of 36.03 W/m^2.

Disposition B experiences a similar situation regarding the interaction between TIR and the sun's altitude angle as disposition A. However, the operating temperature changes affect the electrical output power. To clarify, in May, the lower ambient temperature leads to 10.52 W/m^2 (16.7%) more output electrical power compared to July, even though the altitude of the sun and irradiation intensity are the same in both cases. This is due to the higher PV efficiency at the lower operating temperature in May than in July. The electrical power produced by disposition B is almost twice as much as disposition A, ranging from 63.32 W/m^2 to 92.56 W/m^2.

Disposition A appears to have a higher thermal harvesting potential due to the thermal resistance of the VG. However, it is important to note that the outlet air temperature does not reach a temperature suitable for thermal storage requirements. Moreover, during summer months, the absorbed heat may contribute to heat gain. In contrast, the outlet air from disposition B can serve as a source of fresh air for ventilation. While the temperature may not be sufficiently high, it is still higher than the outside air temperature.

The data obtained from the simulations verified that positioning the VG towards the external environment results in an improvement in the efficiency of thermal output power, while the electrical output power decrease. Additionally, the simulations enable the quantification

Table 6
The CoPVTEG simulation output summary data.

Month	Sun altitude [Deg]	Direct solar irradiation [W/m^2]	VG facing outside (disposition A)				VG facing inside (disposition B)			
			Electrical power [W/m^2]	Thermal power [W/m^2]	Inlet temp. [°C]	Outlet temp. [°C]	Electrical power [W/m^2]	Thermal power [W/m^2]	Inlet temp. [°C]	Outlet temp. [°C]
Jan	15.3	1107	37.64	229.92	20.0	23.3	82.14	172.92	6.0	8.2
Feb	20.7	1182	38.56	240.55	20.0	23.4	86.19	185.12	6.0	8.3
Mar	35.4	1278	37.75	241.45	20.0	23.4	77.94	179.73	9.0	11.3
Apr	46.8	1300	40.43	406.20	20.0	25.8	92.56	311.44	11.0	15.0
May	54.8	1301	36.53	340.14	20.0	24.9	73.84	244.87	15.0	18.2
Jun	58.2	1297	37.05	317.61	20.0	24.6	67.00	226.96	17.0	20.0
Jul	55.3	1292	36.03	348.62	20.0	25.0	63.32	250.43	19.0	22.4
Aug	50.4	1287	43.88	377.02	20.0	25.3	88.20	396.11	18.0	23.1
Sep	35.2	1256	36.98	236.80	20.0	23.4	62.79	174.23	16.0	18.3
Oct	24.6	1203	37.79	248.28	20.0	23.5	70.87	183.42	13.0	15.4
Nov	15.4	1101	37.54	232.48	20.0	23.3	76.58	173.77	9.0	11.2
Dec	11.89	1038	36.92	216.46	20.0	23.1	77.29	163.54	7.0	9.1

of the disparities between the two dispositions and offer crucial insights regarding the outlet air temperature for evaluating configuration performance and energy efficiency.

The concept of solar utilization energy efficiency is defined as the ratio of output electrical and/or thermal power to the total radiative power on the glazing surface. In the histograms illustrated in Fig. 11, the electrical and thermal components of the solar utilization energy efficiency are presented separately for both dispositions in the simulated scenarios. The histogram indicates the impact of TIR during summer. This phenomenon occurs from April 1st to September 15th [24] for the individual lenses in the studied case. The figure indicates a notable increase in energy efficiency during this period, starting in April and continuing through August. This is due to the prismatic lenses' ability to concentrate irradiation on the focal points and, consequently, enhance the performance of the PV cells. Although this shows higher energy efficiency during the summer months, it is worth noting that the primary function of the glazing is to provide daylight during winter times, when the electrical and thermal efficiencies decrease.

Solar utilization energy efficiency is determined by beam direction and heat transfer through the device. As a result, disposition A showed slightly better energy performance with an average of 23.6% and 43.0% in winter and summer, respectively. While disposition B converts solar irradiation with a rate of 21.8% in winter and 39% in summer. Despite this, the simulation results suggest that placing the VG inside offers advantages over placing it outside, which include higher electrical output and the potential application of thermal energy for ventilation. However, it is important to note that disposition A, with the VG facing the external environment, should not be disregarded, as it may be more suitable for cold-dominant climate zones where thermal power is useful as an air heat source year-round.

The study highlights the importance of considering local climate and energy needs when selecting the optimal disposition for CoPVTEG in buildings.

6. Conclusions

Understanding the CoPVTEG concept necessitates the solution of a multi-physics problem that encompasses fluid dynamics, heat transfer, radiation, and electricity. Furthermore, the optical properties of the glazing materials and the quality of the glazing surfaces exert a substantial impact on the outcomes. The inclusion of all the aforementioned intricacies renders the problem complex. In order to ascertain the electrical and thermal performance of CoPVTEG systems while accounting for all of the aforementioned complexities, a computational model has been formulated utilizing FEM. The model's objective is to contribute to the development of the concept as well as the optimization of the detailed design.

In order to reduce computational efforts to an acceptable level, several assumptions were made. Nevertheless, the assumptions result in a decrease in the accuracy of the model's output. To evaluate the reliability of the model, experimental efforts were conducted, including testing a prototype and simulating the same scenarios of experimentations in the model. The resulting output of the model was then compared with the measured parameters obtained from the prototype experiment.

According to the analysis, the model results exhibit a high level of resemblance with the experimental results regarding electrical performance, as measuring output electricity is a straightforward process. However, the model's accuracy in terms of thermal performance fell slightly, primarily due to the complexity of the measuring processes and measurement errors of instruments.

Upon comparing the model output with relevant experimental measurements, it is observed that the model predicts electrical performance with a maximum error of 6%. While the results display not as high reliability as the electrical performance in terms of thermal performance. However, it is expected that the degree of resemblance between the model output and experimental measurements regarding thermal performance will be 99.4% with a 10% error tolerance which is accepted for conducting the device energy performance.

Two configurations of the device have been introduced and computationally analysed. The VG can be oriented either towards the external environment or the interior. The selection of the configuration is a trade-off between higher thermal power production in the former case and a greater electrical output power in the latter. The model quantifies the output powers and reveals that electricity generation in the latter configuration is twice that of the former. The output power range varies from 63.32 W/m^2 to 92.56 W/m^2 when the VG is situated towards the interior, in contrast to a minimum of 36.03 W/m^2 and a maximum of 43.88 W/m^2 in the other configuration.

The CoPVTEG concept exhibits a varying thermal harvesting potential ranging from 216.46 W/m^2 to 406.20 W/m^2 when the VG is situated on the external surface. In contrast, the potential reduces ranging between 163.54 W/m^2 to 396.11 W/m^2 when the VG is positioned towards the interior.

For the studied case which is a glazing unit towards the south in a building in Belfast, UK, the simulation suggests that placing the VG towards the interior is recommended due to the drawbacks associated with locating it outwards, such as increased heat gain during summer and lower electrical power generation. This configuration results in higher electrical output and allows for the application of thermal energy for ventilation. However, this does not imply that the other configuration should be disregarded. In colder climate zones, where thermal power serves as a beneficial air heat source throughout the year, placing the VG on the exterior is more advantageous.

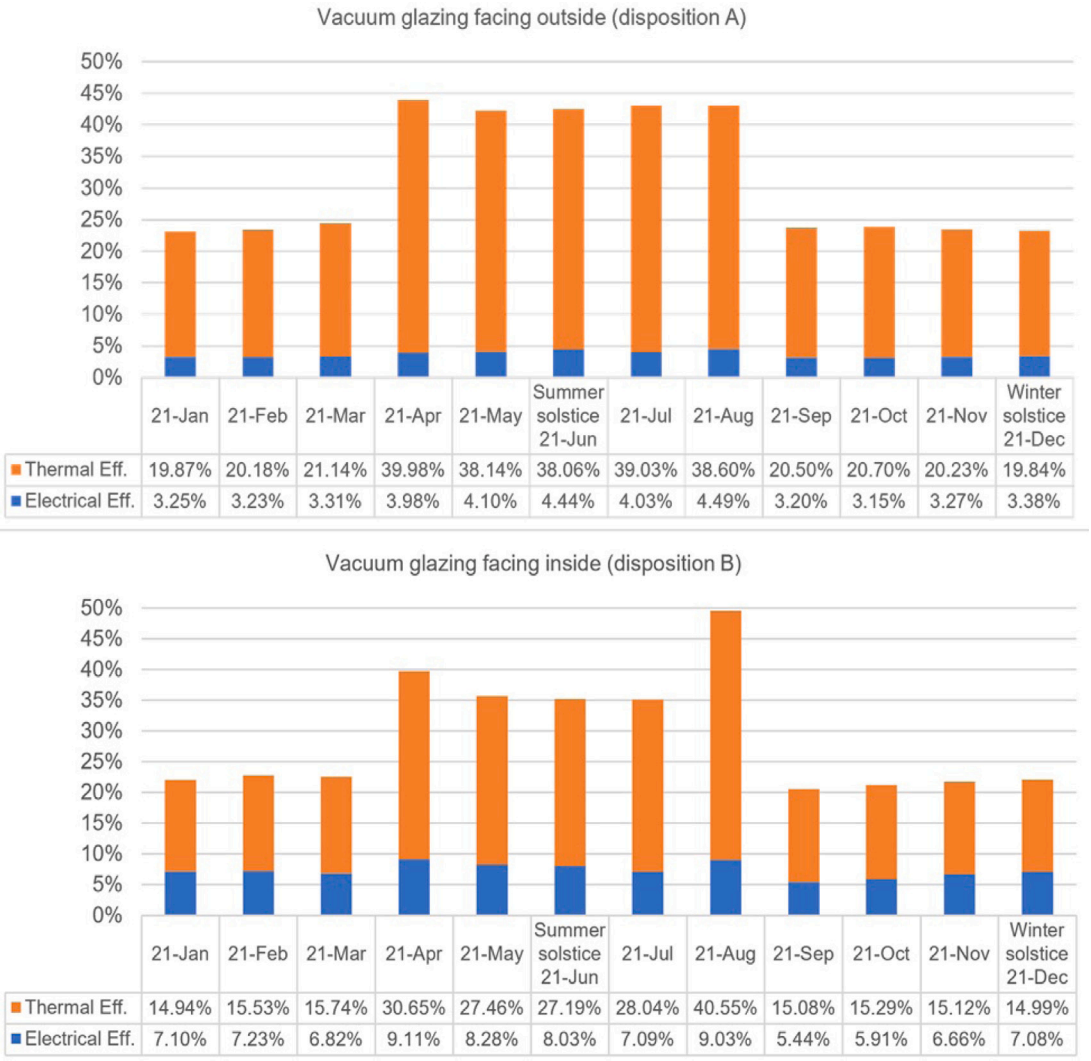

Fig. 11. Solar utilization energy efficiency in the CoPVTEG dispositions.

CRediT authorship contribution statement

Mohammad Ghoraishi: Conceptualization of this study, Methodology, Software, Validation, Investigation, Writing – original draft, Visualization. **Trevor Hyde:** Conceptualization of this study, Methodology, Validation, Formal analysis, Resources, Writing – review & editing, Supervision, Project administration, Funding acquisition. **Aggelos Zacharopoulos:** Conceptualization of this study, Methodology, Validation, Formal analysis, Resources, Writing – review & editing, Supervision, Funding acquisition. **Jayanta Deb Mondol:** Conceptualization of this study, Methodology, Validation, Formal analysis, Resources, Writing – review & editing, Supervision, Funding acquisition. **Adrian Pugsley:** Conceptualization of this study, Methodology, Validation, Investigation, Resources, Data curation, Writing – review & editing, Funding acquisition.

Declaration of competing interest

The authors declare that they have no known competing financial interests or personal relationships that could have appeared to influence the work reported in this paper.

Acknowledgements

This research was undertaken as part of PhD studies funded by VCRS aligned to the Community Energy from Solar Envelope Architecture (CE-SEA) project which was funded by the Centre for Advanced Sustainable Energy (CASE, project number A1109). The authors would like to acknowledge and thank the CE-SEA partners (dpSun Ltd, HHT Renewables Ltd, and Solaform Ltd) for their guidance and support during the project and for their contributions of materials and resources used for realizing the CoPVTG prototype.

References

[1] Energy Consumption in the UK, Department for Business, Energy & Industrial Strategy (BEIS), 2019, Available online: https://www.gov.uk/government/statistics/energy-consumption-in-the-uk (accessed on 22 2023).

[2] UK government, 2021, Available online: https://assets.publishing.service.gov.uk/government/uploads/system/uploads/attachment_data/file/1033990/net-zero-strategy-beis.pdf (accessed on 22 2023).

[3] Reducing UK Emissions 2019, Report CCC/013, Progress Report To Parliament, Committee on Climate Change (CCC), 2019, Available online: https://www.theccc.org.uk/publication/reducing-uk-emissions-2019-progress-report-to-parliament/ (accessed on 14 2023).

[4] A.S. Abdelrazik, Bashar Shboul, Mohamed Elwardany, R.N. Zohny, Ahmed Osama, The recent advancements in the building integrated photovoltaic/thermal (BIPV/T) systems: An updated review, Renew. Sustain. Energy Rev. (ISSN: 1364-0321) 170 (2022) 112988, http://dx.doi.org/10.1016/j.rser.2022.112988.

[5] Aritra Ghosh, Senthilarasu Sundaram, Tapas K. Mallick, Investigation of thermal and electrical performances of a combined semi-transparent PV-vacuum glazing, Appl. Energy (ISSN: 0306-2619) 228 (2018) 1591–1600, http://dx.doi.org/10.1016/j.apenergy.2018.07.040.

[6] Qingdong Xuan, Guiqiang Li, Yashun Lu, Bin Zhao, Fuqiang Wang, Gang Pei, Daylighting utilization and uniformity comparison for a concentrator-photovoltaic window in energy saving application on the building, Energy (ISSN: 0360-5442) 214 (2021) 118932, http://dx.doi.org/10.1016/j.energy.2020.118932.

[7] Qingdong Xuan, Guiqiang Li, Yashun Lu, Bin Zhao, Xudong Zhao, Yuehong Su, Jie Ji, Gang Pei, Design, optimization and performance analysis of an asymmetric concentrator-PV type window for the building south wall application, Sol. Energy (ISSN: 0038-092X) 193 (2019) 422–433, http://dx.doi.org/10.1016/j.solener.2019.09.084.

[8] Wei Zhang, Jianhui Li, Lingzhi Xie, Xia Hao, Tapas Mallick, Yupeng Wu, Hasan Baig, Katie Shanks, Yanyi Sun, Xiaoyu Yan, Hao Tian, Zihao Li, Comprehensive analysis of electrical-optical performance and application potential for 3D concentrating photovoltaic window, Renew. Energy (ISSN: 0960-1481) 189 (2022) 369–382, http://dx.doi.org/10.1016/j.renene.2022.02.121.

[9] Xiao Liu, Yupeng Wu, Design, development and characterisation of a Building Integrated Concentrating Photovoltaic (BICPV) smart window system, Sol. Energy (ISSN: 0038-092X) 220 (2021) 722–734, http://dx.doi.org/10.1016/j.solener.2021.03.037.

[10] Wenwen Guo, Li Kong, Tintai Chow, Chunying Li, Qunzhi Zhu, Zhongzhu Qiu, Lin Li, Yalin Wang, Saffa B. Riffat, Energy performance of photovoltaic (PV) windows under typical climates of China in terms of transmittance and orientation, Energy (ISSN: 0360-5442) 213 (2020) 118794, http://dx.doi.org/10.1016/j.energy.2020.118794.

[11] Zisis Ioannidis, Efstratios-Dimitrios Rounis, Andreas Athienitis, Ted Stathopoulos, Double skin façade integrating semi-transparent photovoltaics: Experimental study on forced convection and heat recovery, Appl. Energy (ISSN: 0306-2619) 278 (2020) 115647, http://dx.doi.org/10.1016/j.apenergy.2020.115647.

[12] Meng Wang, Jinqing Peng, Nianping Li, Hongxing Yang, Chunlei Wang, Xue Li, Tao Lu, Comparison of energy performance between PV double skin facades and PV insulating glass units, Appl. Energy (ISSN: 0306-2619) 194 (2017) 148–160, http://dx.doi.org/10.1016/j.apenergy.2017.03.019.

[13] K.E. Park, G.H. Kang, H.I. Kim, G.J. Yu, J.T. Kim, Analysis of thermal and electrical performance of semi-transparent photovoltaic (PV) module, Energy (ISSN: 0360-5442) 35 (6) (2010) 2681–2687, http://dx.doi.org/10.1016/j.energy.2009.07.019.

[14] Weilong Zhang, Lin Lu, Xi Chen, Performance evaluation of vacuum photovoltaic insulated glass unit, Energy Procedia (ISSN: 1876-6102) 105 (2017) 322–326, http://dx.doi.org/10.1016/j.egypro.2017.03.321.

[15] Yueping Fang, Trevor J. Hyde, Farid Arya, Neil Hewitt, Philip C. Eames, Brian Norton, Seth Miller, Indium alloy-sealed vacuum glazing development and context, Renew. Sustain. Energy Rev. (ISSN: 1364-0321) 37 (2014) 480–501, http://dx.doi.org/10.1016/j.rser.2014.05.029.

[16] Changyu Qiu, Hongxing Yang, Haiying Sun, Investigation on the thermal performance of a novel vacuum PV glazing in different climates, Energy Procedia (ISSN: 1876-6102) 158 (2019) 706–711, http://dx.doi.org/10.1016/j.egypro.2019.01.190.

[17] Junchao Huang, Xi Chen, Hongxing Yang, Weilong Zhang, Numerical investigation of a novel vacuum photovoltaic curtain wall and integrated optimization of photovoltaic envelope systems, Appl. Energy (ISSN: 0306-2619) 229 (2018) 1048–1060, http://dx.doi.org/10.1016/j.apenergy.2018.08.095.

[18] H. Jarimi, K. Qu, S. Zhang, Q. Lv, J. Liao, B. Chen, H. Lv, C. Cheng, J. Li, Y. Su, S. Dong, S. Riffat, Performance analysis of a hybrid thin film photovoltaic (PV) vacuum glazing, Future Cities Environ. 6 (1) (2020) 2, http://dx.doi.org/10.5334/fce.73.

[19] Hasila Jarimi, Qinghua Lv, Omar Ramadan, Shihao Zhang, Saffa Riffat, Design, mathematical modelling and experimental investigation of vacuum insulated semi-transparent thin-film photovoltaic (PV) glazing, J. Build. Eng. (ISSN: 2352-7102) 31 (2020) 101430, http://dx.doi.org/10.1016/j.jobe.2020.101430.

[20] Aritra Ghosh, Nabin Sarmah, Senthilarasu Sundaram, Tapas K. Mallick, Numerical studies of thermal comfort for semi-transparent building integrated photovoltaic (BIPV)-vacuum glazing system, Sol. Energy (ISSN: 0038-092X) 190 (2019) 608–616, http://dx.doi.org/10.1016/j.solener.2019.08.049.

[21] Changyu Qiu, Yun Kyu Yi, Meng Wang, Hongxing Yang, Coupling an artificial neuron network daylighting model and building energy simulation for vacuum photovoltaic glazing, Appl. Energy (ISSN: 0306-2619) 263 (2020) 114624, http://dx.doi.org/10.1016/j.apenergy.2020.114624.

[22] Zacharopoulos, Aggelos (Inventor), Mondol, Jayanta Deb (Inventor), Hyde, Trevor (Inventor), et al., Concentrating Evacuated Photovoltaic Glazing Panel, Patent No.: PCT/GB2011/050327, 2010.

[23] A. Zacharopoulos, J. Mondol, M. Smyth, T. Hyde, A. Pugsley, Investigation of the thermal performance of a concentrating PV/Thermal glazing façade technology, in: BIRES 2017 - Proceedings, First International Conference on Building Integrated Renewable Energy Systems (BIRES 2017), European Cooperation in Science and Technology, Dublin, Ireland, 2017, Paper 64, 6/03/17.

[24] Ghoraishi Mohammad, Trevor Hyde, Aggelos Zacharopoulos, Jayanta Deb Mondol, Adrian Pugsley, Experimental characterization of the optical performance of concentrating photovoltaic glazing (CoPVG) systems, Energies 16 (6) (2023) 2891, http://dx.doi.org/10.3390/en16062891.

[25] Giovanni Barone, Aggelos Zacharopoulos, Annamaria Buonomano, Cesare Forzano, Giovanni Francesco Giuzio, Jayanta Mondol, Adolfo Palombo, Adrian Pugsley, Mervyn Smyth, Concentrating PhotoVoltaic glazing (CoPVG) system: Modelling and simulation of smart building façade, Energy (ISSN: 0360-5442) 238 (2022) 121597, http://dx.doi.org/10.1016/j.energy.2021.121597, Part B.

[26] Giovanni Barone, Annamaria Buonomano, Roma Chang, Cesare Forzano, Giovanni Francesco Giuzio, Jayanta Mondol, Adolfo Palombo, Adrian Pugsley, Mervyn Smyth, Aggelos Zacharopoulos, Modelling and simulation of building integrated Concentrating Photovoltaic/Thermal Glazing (CoPVTG) systems: Comprehensive energy and economic analysis, Renew. Energy (ISSN: 0960-1481) 193 (2022) 1121–1131, http://dx.doi.org/10.1016/j.renene.2022.04.119.

[27] S. Pantic, L. Candanedo, A.K. Athienitis, Modeling of energy performance of a house with three configurations of building-integrated photovoltaic/thermal systems, Energy Build. (ISSN: 0378-7788) 42 (10) (2010) 1779–1789, http://dx.doi.org/10.1016/j.enbuild.2010.05.014.